ACS APPLIED MATERIALS & INTERFACES

Research Article

www.acsami.org

Palladium−Silver-Activated ZnO Surface: Highly Selective Methane Sensor at Reasonably Low Operating Temperature

Sugato Ghosh,[†] Chirasree RoyChaudhuri,[‡] Raghunath Bhattacharya,[†] Hiranmay Saha,*[,†] and Nillohit Mukherjee*[,†]

[†]Centre of Excellence for Green Energy and Sensor Systems, Bengal Engineering and Science University, Howrah 711103, West Bengal, India

[‡]Department of Electronics and Telecommunication Engineering, Bengal Engineering and Science University, Howrah 711103, West Bengal, India

Supporting Information

ABSTRACT: Metal oxide semiconductors (MOS) are well known as reducing gas sensors. However, their selectivity and operating temperature have major limitations. Most of them show cross sensitivity and the operating temperatures are also relatively higher than the value reported here. To resolve these problems, here, we report the use of palladium−silver (70−30%) activated ZnO thin films as a highly selective methane sensor at low operating temperature (~100 °C). Porous ZnO thin films were deposited on fluorine-doped tin oxide (FTO)-coated glass substrates by galvanic technique. X-ray diffraction showed polycrystalline nature of the films, whereas the morphological analyses (field emission scanning electron microscopy) showed flake like growth of the grains mainly on xy plane with high surface roughness (107 nm). Pd−Ag (70−30%) alloy was deposited on such ZnO films by e-beam evaporation technique with three different patterns, namely, random dots, ultrathin (~1 nm) layer and thin (~5 nm) layer as the activation layer. ZnO films with Pd−Ag dotted pattern were found show high selectivity towards methane (with respect to H_2S and CO) and sensitivity (~80%) at a comparatively low operating temperature of about 100°C. This type of sensor was found to have higher methane selectivity in comparison to other commercially available reducing gas sensor.

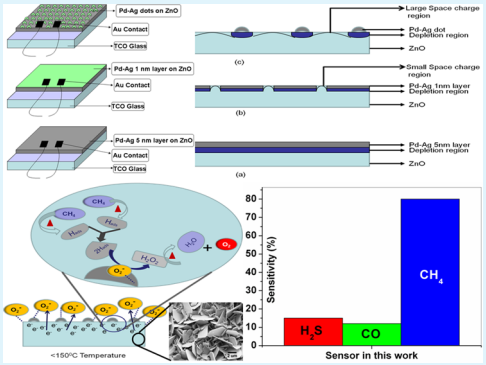

KEYWORDS: *palladium−silver, surface activation, ZnO thin films, methane sensor, high selectivity, low operating temperature*

1. INTRODUCTION

In recent years, metal oxides (MO), such as ZnO, SnO_2, and WO_3, have been widely used for the detection of flammable, explosive, and toxic gases (like methane, hydrogen sulfide, carbon monoxide, etc.) because of their unique sensing properties like resistivity change in presence of target gases, response and recovery time.[1−5] Among them, ZnO is an n-type semiconductor that exhibits an excellent sensing property with high electrochemical stability and non toxicity.[6] The band gap energy of ZnO lies typically between 3.1 and 3.4 eV. One dimensional (1D) structures like nanowires,[7] nanorods,[8] nanobelts,[9] and two dimensional (2D) structure, such as nanoplates,[10,11] are becoming the subject of interest for scientists because of their small size and high surface-to-volume ratio, which help them to detect gases with a wide range of concentrations by lowering the limit of detection.

It is believed that, the change in electrical properties of the metal oxide semiconductors (MOS) happens because of the adsorption of gas molecules and primarily concerned with the chemisorption of the oxygen on the surface. Molecular oxygen is first adsorbed from air on the surface of the MOS and then dissociates to form O^- and O^{2-} ions, which can be described using eq 1.

$$(\beta/2)O_{2(gas)} + \alpha e^- + S \leftrightarrow O^{\alpha-}{}_{\beta(S)} \quad (1)$$

Where S denotes the unoccupied chemisorption sites for oxygen and $O^{\alpha-}_{\beta(S)}$ is the chemisorbed oxygen with $\alpha = 1$ or 2 for singly or doubly ionized form and $\beta = 1$ or 2 for atomic or molecular form, respectively. The electrons are extracted from the conduction band of the *n*-type semiconductor which creates a depletion or space charge layer on the surface of the MOS, which in turn induces band bending. Thus, the adsorbed oxygen plays a vital role to decrease the resistance of the MOS in presence of the combustible/reducing gas. This phenomenon may be explained by the eq 2.

Received: November 2, 2013
Accepted: February 24, 2014
Published: February 24, 2014

$$e^- + O_2 \leftrightarrow O_2^-$$
$$e^- + O_2^- \rightarrow 2O^-$$
$$R + O^- \rightarrow RO + e^- \quad (2)$$

Where R is the reducing gas, which reacts with O^- and releases the electron e^- by forming the oxide RO.

A number of metal oxides have been reported in the published literature for the detection of different gases, for example, ZnO has been reported for the detection of hydrocarbon,[12−17] carbon monoxide[18−20] and ammonia,[21−23] however, most of them have concentrated on extending the sensitivity of the sensors for different analytes. Bhattacharyya et. al.[16] have reported the use of Si supported ZnO nanostructures along with Pd−Ag surface modification for methane sensing with highest sensitivity of 73% at an operating temperature not less than 175 °C. Hsueh et. al.[14] reported the fabrication and application of laterally grown ZnO nanowires as the ethanol vapor sensor, however, their highest sensitivity was 61% at an operating temperature of 300 °C. On the other hand, modified ZnO nanowires can also be used for detection of CO as reported by Hsueh et. al.,[14] however, their reported maximum sensitivity was 57% at 320 °C. Fe_2O_3−ZnO nanocomposite was also found to be an excellent candidate for the selective detection of ammonia at room temperature.[23] It is to be noted that methane is a highly flammable gas which is commonly found in underground coal mines as well as inside the manholes in high concentration (1%), and a small spark can cause a violent explosion if the concentration exceeds the threshold limit. Therefore, the detection of high concentration methane at a low operating temperature (without raising any false alarm) is of great importance from the view point of both environmental protection and human health.

MOS-based sensors are generally found to be sensitive to the host of the analyte or a series of analytes with similar physicochemical properties, and there lies the problem. The use of different types of metals, such as Pd,[24,25] Pt,[26] Au,[27] Ag,[28−30] Cu,[31] Co,[32] non-metals, such asF,[33] or metal oxides, such as CuO, as additives are quite common for he purpose of increasing sensitivity. The use of such additives in turn increases the cross-sensitivity and hence, the selectivity is lowered. This may lead to some false positive signal. On the other hand, the use of metal alloys instead of metals to enhance the selectivity, as well as sensitivity, at a reasonably low operating temperature has not been reported so far to the best of our knowledge. However, Moon et. al.[34] have reported the fabrication of ZnO nanowhisker-based methane sensor activated by Pd−Ag layer for the enhancement of sensitivity at reduced operating temperature. Also, the commercially available MOS-based sensors operating in resistive mode are found to have reasonable sensitivity but adequately low selectivity.

The good thing with ZnO, which has been chosen as the base material here, is that, it can be synthesized in the form of both thin and thick films by various techniques like sputtering,[35−37] chemical vapor deposition,[38−40] thermal evaporation,[41] metal organic chemical vapor deposition,[42] electron beam evaporation,[43] pulsed laser deposition,[44] sol−gel,[45−47] arc plasma reaction,[48] etc. In this work, we have considered a modified electrochemical technique, called the galvanic technique,[49,50] for the deposition of ZnO thin films on transparent conducting oxide (TCO) coated glass substrates. To increase the sensitivity and selectivity of CH_4, the authors have experimented with e-beam evaporated Pd−Ag alloy to form a bilayer structure. The Pd−Ag alloy has been deposited on ZnO films in two ways, namely, uniform deposition of ultrathin layer without using mask and dotted structure using a mask.

This work includes the use of Pd−Ag alloy for the first time to enhance the selectivity (among CH_4, H_2S, and CO) as well as sensitivity at a reasonably low operating temperature (~100°C). Most of the previous works reported response above 300 °C[51,16,17] which is not desirable in mining environment. Here, the response characteristics were measured for bare ZnO, ZnO/Pd−Ag alloy ultrathin layer (1 and 5 nm), and ZnO/Pd−Ag alloy dotted structure in presence of methane, carbon monoxide and hydrogen sulfide. A commercially available MOS type methane sensor was also exposed to the same gaseous environment, to compare the performance. We have also tried to find out the actual reason and the related reaction mechanism behind such enhanced selectivity.

2. EXPERIMENTAL SECTION

2.1. Synthesis of Porous ZnO Films. ZnO thin films with flakelike morphology were deposited using a modified electrochemical technique, called galvanic technique. The detailed deposition procedure has been published elsewhere.[49,50] It has been found that the flake like growth of the ZnO grains mainly on xy plane resulted in porous structure with high surface roughness, which in turn, helps in better adsorption of the test gases. So, in this work, we have carried out the surface activation and sensing experiments on the ZnO films with flake like morphology distributed on *xy* plane.

2.2. Deposition of Pd−Ag Alloy on the Surface of ZnO Thin Films. Commercially available Pd−Ag alloy (70% Pd and 30% Ag) was deposited on the ZnO film surface with three different structures using electron beam evaporation technique (Auto 500, Hind High Vac). In the first structure, Pd−Ag dots were deposited on the ZnO surface through an aluminium (foil) mask having an average pore diameter of 0.5 mm. In the second and third case, 1 and 5 nm thin layers of Pd−Ag alloy were deposited on the ZnO films, respectively. Both in second and third technique, no mask were used. For all cases, the e-beam evaporation was carried out at 4×10^{-6} mbar of pressure. The thickness of films was monitored using an inbuilt dynamic thickness monitor. To make ohmic electrical contacts with the sensing layer, metallic Au was evaporated by e-beam technique. The area of each metal pad was 0.1 mm ×0.1 mm on which conducting wires were connected using bonding machine. As the effective area of such Au contacts was significantly small in comparison to the entire sensor surface, it is expected that the influence of these Au pads towards the sensing mechanism of the proposed sensor prototype will be negligible. The schematic of the process is shown in Scheme 1.

2.3. Analysis Techniques. The morphology and crystal structure of ZnO films were analyzed by field-emission scanning electron microscope (FESEM, Carl Zeiss) and X-ray diffraction (XRD, SEIFERT 3000P, parallel beam geometry, Bragg-Brentano goniometer, source Cu Kα, λ = 1.540598 Å) techniques, respectively. The optical measurements were carried out using a JASCO V-530 UV-Vis unit. The gas sensing properties of the developed sensor prototypes and some commercially available sensors have been measured by a gas analyzing system as shown in Scheme 2 and a comparative analysis of their properties has been carried out. The flow of the gases inside the mixing chamber was controlled by mass flow controllers (MFC, MKS Inc., model 1479A). IOLAR grade N_2 was used as the carrier gas. The mass flow rate and thus the relative concentration of the gases were kept constant throughout the experiment. The developed and procured sensors were exposed in three types of gases, namely, CH_4, H_2S, and CO. The sensing performance was measured by "resistive mode" and the sensitivity in percentage (S) was calculated as

$$S = [(R_a - R_g) \times 100]/R_a$$

Scheme 1. Schematic of the Three Proposed Sensor Structures

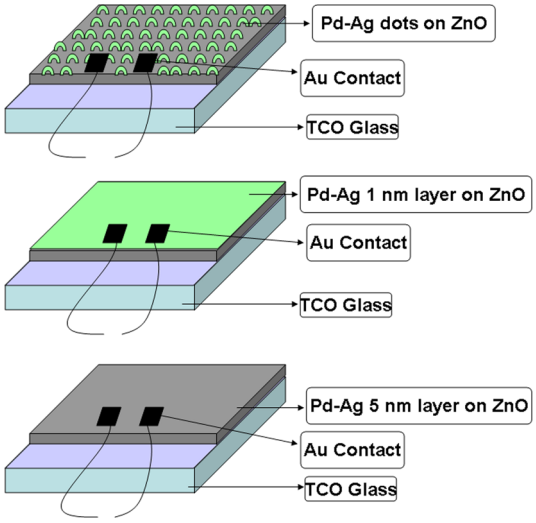

where iR_a is the sensor resistance in air and R_g is the corresponding resistance in presence of the test (reducing) gas.

3. RESULTS AND DISCUSSION

3.1. Structural Characterization by XRD. X-ray diffraction measurements of the films were carried out to ascertain the formation of ZnO and to determine the phase and grain growth. The thickness of the film taken for XRD analysis was about 0.60 μm. From the XRD pattern (Figure 1), the deposition of polycrystalline (with no preferred orientation to any particular crystallographic plane) ZnO films was observed. The diffractions were observed from eight crystallographic planes, namely, (100), (002), (101), (102), (110), (103), (112), and (202), which indicate the formation of wurtzite (hexagonal) ZnO and matched well with the standard diffraction pattern (JCPDS card no. 05-0664). Among all the crystallographic planes, the highest intensity was observed for the (101) plane. The asterisk-marked peaks in the XRD pattern represent SnO_2 of the bottom FTO substrate (JCPDS card no. 21-1250). The sharp diffraction peaks indicate significant crystallinity, which in turn helps in better device performance.

3.2. Morphological Analyses by FESEM. The FESEM image of the uncoated film is shown in Fig. 2a, from which a randomly oriented hexagonal flakelike morphology for the deposited films is observed. The hexagonal geometry of the

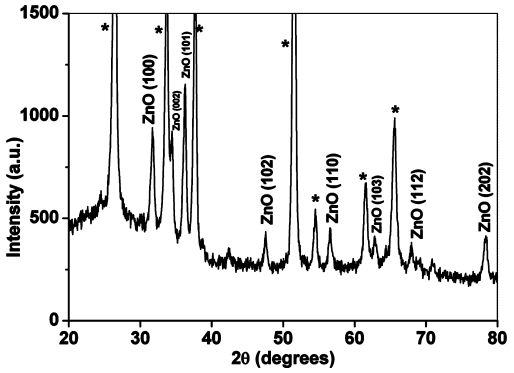

Figure 1. XRD pattern of the deposited ZnO film.

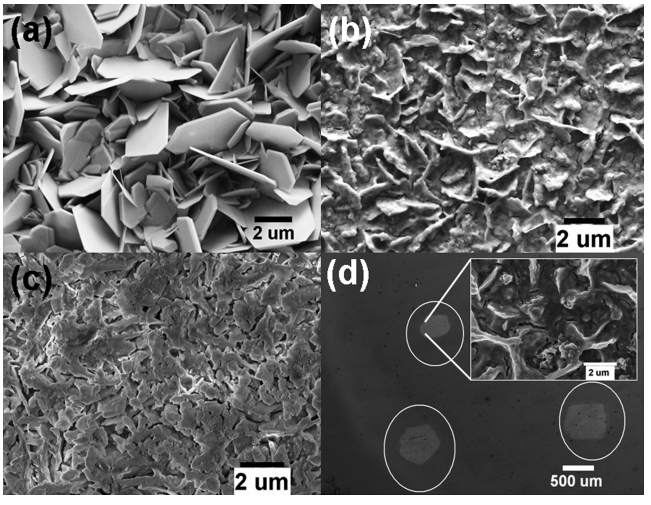

Figure 2. FESEM images of (a) blank ZnO film, (b) ZnO film with 1 nm Pd–Ag coating, (c) ZnO film with 5 nm Pd–Ag coating, and (d) Pd–Ag dots. Inset: High magnification image showing the morphology of a dot.

films supports the findings from XRD analysis. Such a random orientation of the flakelike grains makes the surface significantly rough which also consists numerous hollow cages formed by the overlapping of the grains and sufficient amount of exposed surface area on the grains. These factors, mainly the enhanced active surface area, help in better adsorption of the gaseous species and device performance. The average thickness of such hexagonal grains was found to be about 200 nm, while the length of a side was about 3 μm. When a 1 nm thin layer of

Scheme 2. Illustration of the Gas Flow and Measurement System

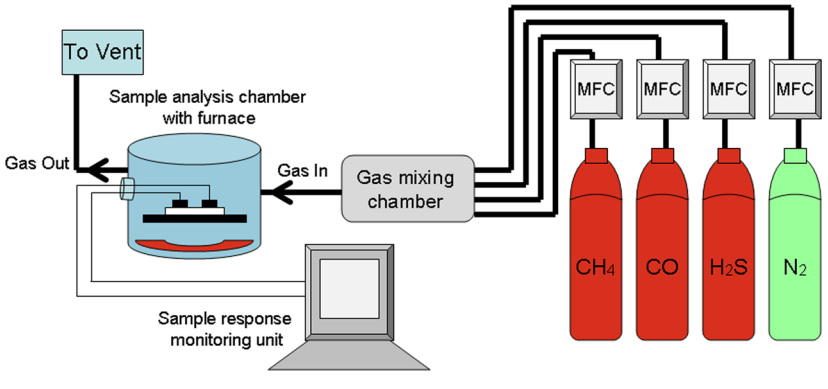

dx.doi.org/10.1021/am404883x | ACS Appl. Mater. Interfaces 2014, 6, 3879–3887

Pd−Ag was deposited on the ZnO films, the morphology becomes to some extent smoother, as can be seen from Figure 2b. The hollow cages were found to be filled up partially by the alloy giving rise to a ridge-and-valley topography. Some clusters of the alloy on the valley can also be seen from Figure 2b. The surface becomes further smoother on depositing a 5 nm thin layer of Pd−Ag alloy (Figure 2c) as most of the hollow cages were found to be filled up by the alloy evaporation, giving rise to a porous but flat structure. Figure 2d is showing the dotted pattern of the deposited Pd−Ag alloy. The high magnification image of a dot (Fig.2d inset) is showing similar ridge-and-valley structure as obtained for the 1 nm thin alloy coating. This indicates sufficient unevenness within a dot.

3.3. Optical Properties. To have an idea about the band gap energy of the deposited material, UV-Vis measurements were carried out. The absorption spectrum (Figure 3) shows a sharp raise around 400 nm which corresponds to the band gap energy of about 3.1 eV, typical for bulk ZnO at room temperature. The sharp increase in the absorption spectra, in its turn, reflects good crystalline nature of the deposited film, which is in good agreement with the XRD analysis.

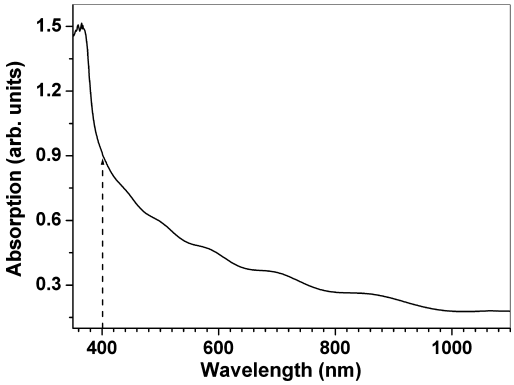

Figure 3. UV−vis absorption spectrum of representative blank ZnO film.

3.4. Selective Methane Sensing. The sensing properties of different types of sensor prototypes developed in this work were measured in presence of diluted CH_4, H_2S, and CO. The concentration of each gas and the temperature of the experiment were maintained at ∼1% (with a tolerance of 0.2% of full scale) and 100 °C (± 2 °C), respectively and the flow rate of each gas was maintained at 35 sccm throughout the whole experiment. The sensor chamber was purged with dry nitrogen and air, initially and after each set of measurements. After the samples were loaded, the measurement chamber was closed; the vent valve was opened and the chamber was purged with dry nitrogen and dry air until it reaches the operating temperature of 100 °C (approximate duration 15 minutes). As soon as the dry air and nitrogen started flowing over the surface of the sensor, the ZnO layer starts trapping the oxygen from the purged air and forms O^{2-}. When the optimum operating temperature was reached, purging of dry air and nitrogen was stopped and the test gas with required concentration was allowed to flow in to the chamber for 3 minutes and the measurement was carried out. After the data were recorded, the inflow of test gas was stopped and the chamber was again purged with dry air and nitrogen until the initial resistance was recovered. During this process, the ZnO layer again traps oxygen from the purged air, forms O^{2-}, and gets ready for the next cycle of operation. To compare the performance of the developed sensor prototypes, commercially available methane sensors were also tested under the same environment. The response of the developed ZnO/Pd−Ag dotted sensor prototype at 100 °C showed a stable response and high sensitivity towards methane. For H_2S and CO, no such high level of sensitivity was observed, which indicates a specific level of selectivity of this prototype towards methane. The sensing results and the recovery of ZnO/Pd−Ag dot type sensor prototype for CH_4, H_2S, and CO are shown in Figure 4a. A fall of resistance of about 200 KΩ (initial 250 KΩ, final 50 KΩ) was observed for CH_4 after 300 s for the dotted prototype. The change was insignificant for H_2S and CO. The response of the commercially available MOS based sensor towards the three test gases under the same condition is shown in Fig. 4b, which reveals almost similar type of response for CH_4, H_2S, and CO, making it poorly selective towards CH_4. Its first response time was relatively short; however, the response ratio curve starts deteriorating after repeated exposure towards the test gases. This might be due to the similar adsorption mechanism exerted by the commercially available sensor towards the three test gases, which is not desirable. The response curves towards 1% CH_4 for ZnO/Pd−Ag 1 nm layer and ZnO/Pd−Ag 5 nm layer structures are shown in Figure 4c and 4d, respectively, which revealed almost similar trend. A fall of resistance of about 100 KΩ (initial 180 KΩ, final 80 KΩ) and 70 KΩ (initial 150 KΩ, final 80 KΩ) were observed for CH_4 after 7 and 9 s for the 1 and 5 nm layered structure, respectively. As these performances towards only methane are comparatively poor, we did not carry out any selectivity measurements with these two patterns. Figure 5a indicates good repeatable response characteristics for all the three developed sensor prototypes for methane gas. It was also found that the ZnO/Pd−Ag 5 nm layer sensors have 40%, ZnO/Pd−Ag 1 nm layer sensors have 50% and ZnO/Pd−Ag dotted sensors have 80% (highest among the three) response towards methane. A comparative bar diagram of response and cross sensitivity for procured methane sensor and ZnO/Pd−Ag dotted sensor is shown in Fig. 5b. The procured sensor showed a response more than 90% for all three gases, without any selectivity, where as ZnO/Pd−Ag dotted sensor showed 80% response selectively towards methane and only 12% and 15% response towards CO and H_2S, respectively, at an operating temperature of 100°C. This indicates high selectivity and sensitivity of the Pd−Ag dotted pattern towards methane in comparison to the commercially available sensor.

To evaluate the stability and repeatability of the fabricated sensor, a five-day long experiment with 10 cycles per day, leading to total 50 cycles, were carried out, which is shown in Figure 5c. The sensor performance was found to be consistent throughout the 50 cycles, however, slight decrease in sensitivity was observed during the last 10 cycles on the fifth day, which might be due to the trapping of the test gas and less degassing occurred after so many cycles of test, which is natural for MOS based gas sensors. However, the results are promising as they fall within the acceptable limit.

The concentration dependent nature of the proposed sensor for CH_4, CO, and H_2S is shown in Figure 5d. The measurements were carried out over a concentration range of 0.1% to 1.0% of the three test gases and the fabricated sensor was found to be highly selective to CH_4 over this wide range of concentration. However, the methane sensitivity was found to increase with an increase in the concentration of the gas, but this trend was not so prominent for CO and H_2S. The order of

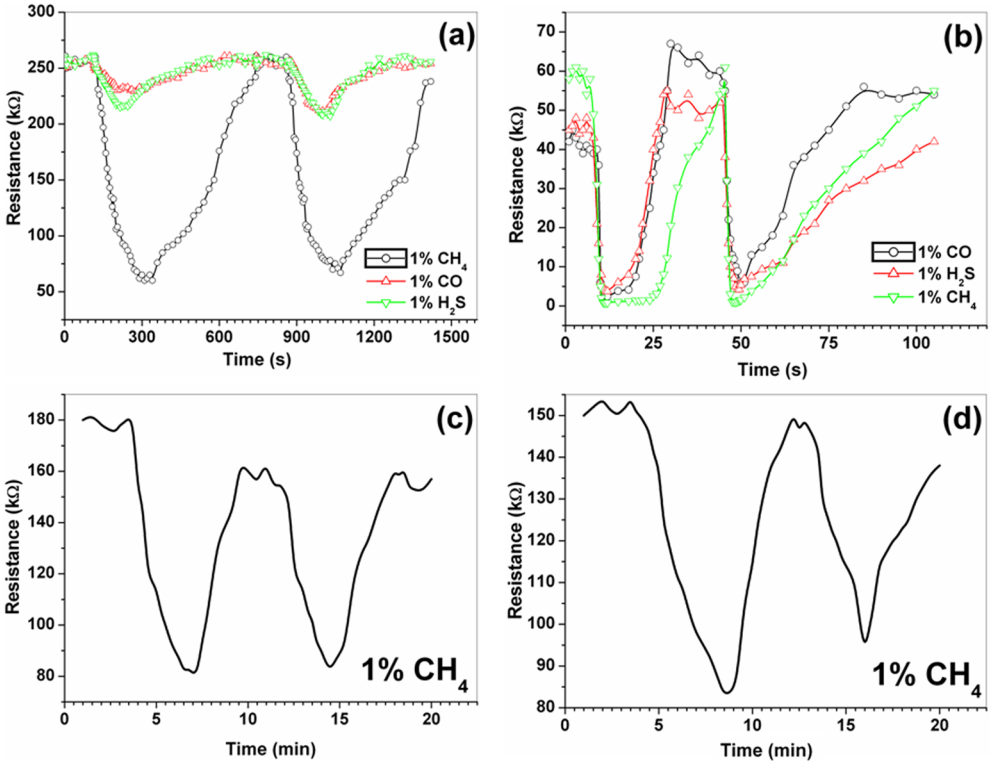

Figure 4. Response curves for (a) ZnO/Pd−Ag dot type sensor prototype towards 1% CH_4, H_2S, and CO, (b) procured sensor towards 1% CH_4, H_2S, and CO, (c) ZnO/Pd−Ag 1 nm layer towards 1% CH_4, and (d) ZnO/Pd−Ag 5 nm layer towards 1% CH_4. The operating temperature was 100 °C for all measurements.

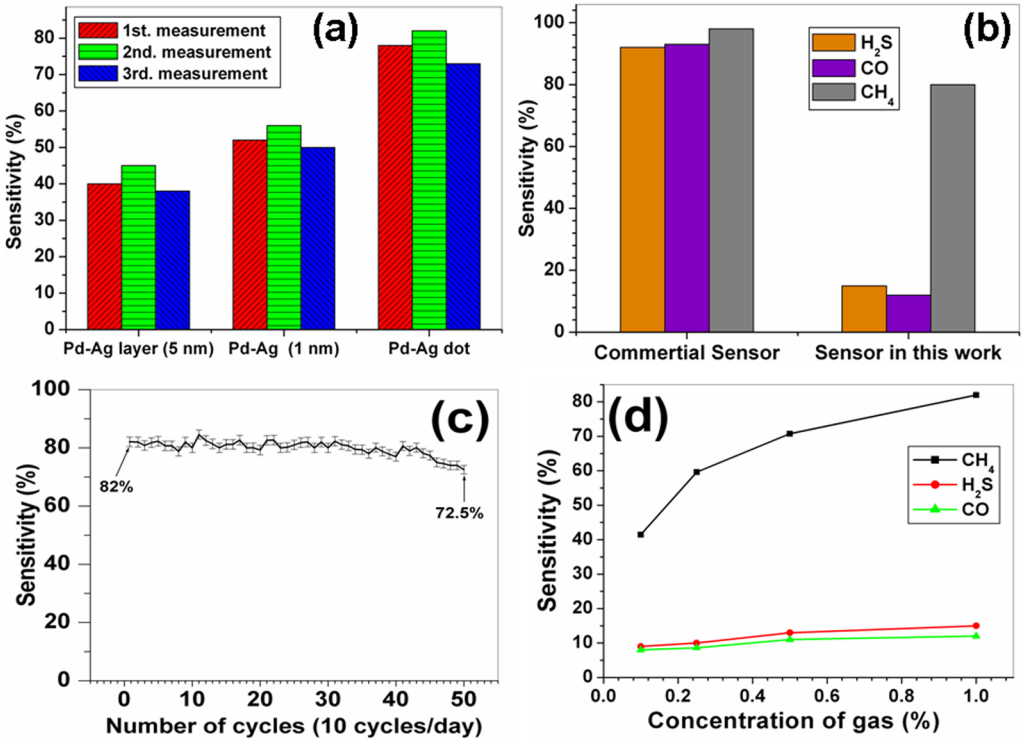

Figure 5. (a) Bar diagrams showing repeatability of the developed sensor prototypes towards 1% methane, (b) comparative bar diagram of response and cross sensitivity for the procured sensor and the developed ZnO/Pd−Ag dotted sensor, (c) number of cycles vs. sensitivity plot showing the stability of the ZnO/Pd−Ag dotted sensor, and (d) variation of sensitivity of the ZnO/Pd−Ag dotted sensor with the concentration of the test gases at 100 °C.

methane sensitivity was about 42 > 60 > 71 > 82% for 0.1, 0.25, 0.50, and 1.0% of the gas, respectively. The results also indicate that the proposed sensor prototype is quite eligible to detect CH_4 selectively from a mixture of CH_4, CO, and H_2S over a

dx.doi.org/10.1021/am404883x | ACS Appl. Mater. Interfaces 2014, 6, 3879−3887

Scheme 3. Mechanism for Oxygen Absorption on the Pd−Ag Dotted ZnO Surface at (a) Room Temperature, (b) <150 °C, and (c) >150 °C and (d) Methane Sensing Mechanism on the Pd−Ag Activated ZnO Surface at <150°C

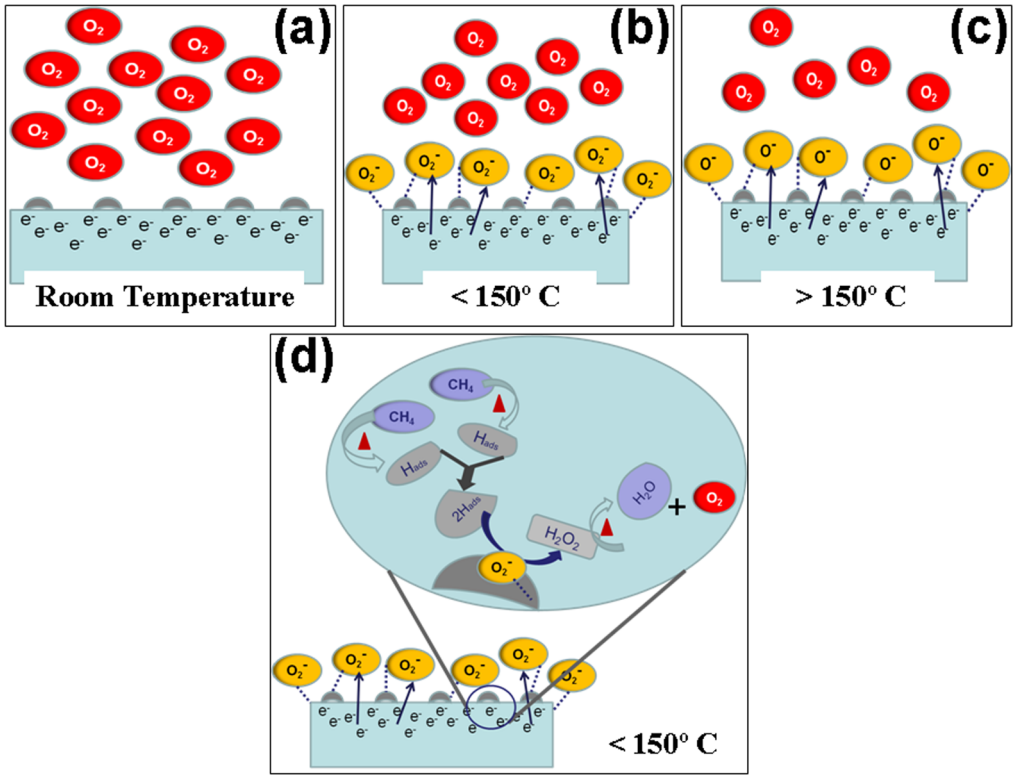

wide range of concentration, which is required for its practical use in coal mines and manholes.

3.5. Mechanism of Selective Methane Sensing by the ZnO/Pd−Ag Dotted Structure. The basic methane sensing mechanism of the ZnO based sensor is supposed to be highly dependent on the adsorbed O_2 molecules on its surface. Basically, one oxygen molecule attracts one electron from the conduction band of *n*-ZnO and forms O_2^-. This reaction takes place at room temperature and O_2^- persists up to 150 °C. Above 150 °C the so formed O_2^- takes up another electron from the conduction band of *n*-ZnO, leading to the formation of O^- ion.[52−55] These O_2^- or O^- ions get adsorbed on the ZnO surface forming ZnO:O_2^-/O^- species through strong ZnO−O_2^-/O^- interaction. When some catalytic metal atom like Pd−Ag, as the case here, is introduced on the surface, same reduction reactions of adsorbed oxygen takes place. (Scheme 3) However, in this case, the majority of the O_2^- ions (as the operating temperature is 100°C for the developed prototype) are bonded with the metal atoms (Pd−Ag) and forms Pd−Ag:O_2^-. As, the strength of such Pd−Ag:O_2^- bond is weaker than ZnO:O_2^- bond,[52,56] so the oxygen species is easily releasable from the metal atoms at comparatively lower temperature. Further, at the operating temperature ∼100°C, CH_4 breaks down to produce $\dot{C}H_3$ and $\dot{H}$.[52,56] This hydrogen radical reacts with the absorbed O_2^- mainly coupled with Pd−Ag, and as a first byproduct we get hydrogen peroxide (H_2O_2). But H_2O_2 is highly unstable at 100°C, so, it breaks down instanteniously in to H_2O and O_2. Gibb's Free energy for formation of $H_2O_{2\,(g)}$ is -105.48 kJ/mol and the breaking up of $H_2O_{2(g)}$ to $H_2O_{(g)}$ and $O_{2(g)}$ is −228.61 kJ/mol. In both cases, the value is negative, indicating the spontaneity of the reaction. Scheme 3 is describing the whole sensing mechanism, where, for the first time the formation of H_2O_2 as the byproduct is reported. Because of the probability of H_2O_2 formation, we got a high response at low operating temperature.

Also for the selectivity enhancement, the absorbed oxygen species play an important role, as the availability of O_2^- and O^- differs at two different operating temperatures. The developed sensor prototypes were very less sensitive towards CO and H_2S, in comparison to CH_4. Such behavior can be explained if we consider the corresponding sensing mechanism. The redox reactions, which might be involved in the detection of CH_4, CO, and H_2S by the metal oxide based sensors, are as follows: (i) $CH_4 \rightarrow \dot{C}H_3 + \dot{H}$, $2\dot{H} + O_2^- \rightarrow [H_2O_2] \rightarrow H_2O + O_2$, (ii) $CO + O^- \rightarrow CO_2 + e^-$, and (iii) $H_2S + O^- \rightarrow SO_2 + H_2O$.[52,57] It can be seen that, CO and H_2S could not react with O_2^- because of the unavailability of vacant orbitals on carbon and high breakdown temperature for H_2S (above 300 °C).[57] It has been mentioned earlier that at about 100 °C, mainly O_2^- ions prevail; along with a diminutive population of O^- ions. This means, at an operating temperature of 100 °C (the case here), mainly CH_4 could undergo the required redox reaction, and hence, be detected. Reaction of CO and H_2S with the diminutive amount of O^- available at 100°C is reflected in the diminished sensitivity of CO and H_2S for the reported prototype, as can be seen from Figure 5b.

3.6. Methane Sensing Mechanism of Different ZnO/Pd−Ag Patterns. In this work, three different patterns of Pd−Ag alloy were deposited on the ZnO thin film surface and three different responses were obtained. An explanation of such behavior has been provided from the point of view of their band structure. The work function of *n*-ZnO (Φ_s) is 4.45 eV and Pd is 5.12 eV (Φ_m).[58,59] The work function of Ag is 4.72 eV, so there is a probability that the effective work function of the Pd−Ag alloy will be lowered by a small amount from that of pure Pd, however, this will still be sufficiently higher than that

dx.doi.org/10.1021/am404883x | ACS Appl. Mater. Interfaces 2014, 6, 3879−3887

Scheme 4. Band Diagram of ZnO and Pd−Ag Alloy (a) before and (b) after Contact at Equilibrium Condition

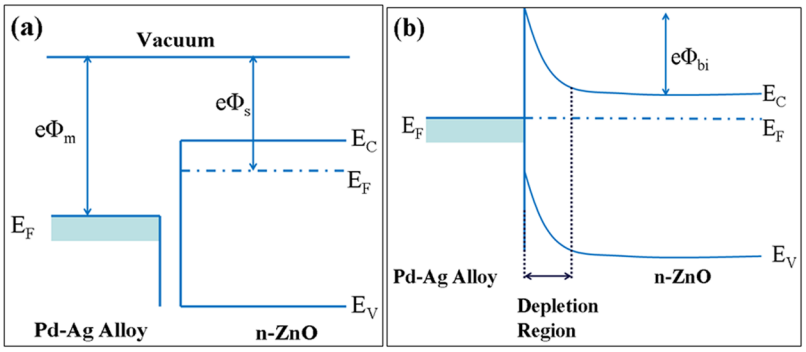

Scheme 5. Schematic of Depletion Region and Space Charge Region Formation for the (a) 5 nm Layer, (b) 1 nm Layer, and (c) Pd−Ag Dotted Structure on the ZnO Surface

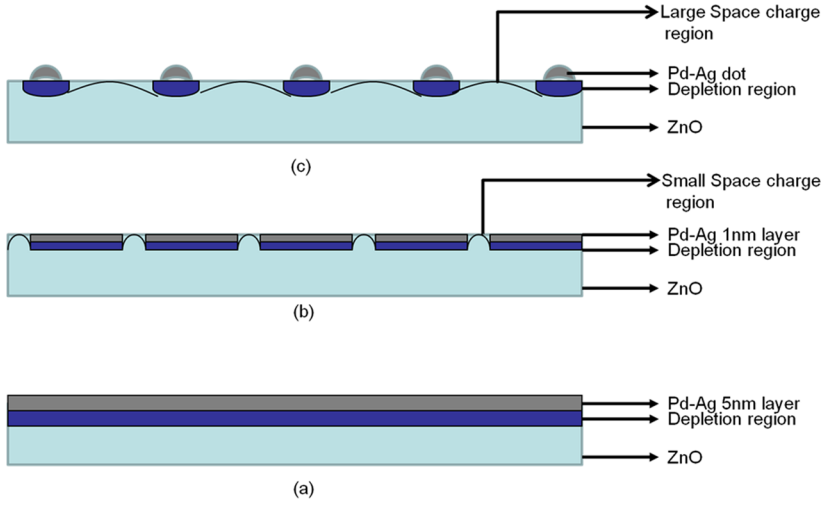

of ZnO. As $\Phi_m > \Phi_s$ we may consider that *n*-ZnO and Pd−Ag metal interface makes a Schottky junction. Because of the formation of junction, a depletion region is created at the interface of the two layers, which is shown in Scheme 4. As a result, the effective thickness of ZnO layer decreases and hence it creates an impression on the internal resistance of it. This may be demonstrated by the following equation:

$$R = \rho \times L/A$$

Where R denotes the resistance of the film, ρ is resistivity, iL denotes the distance between two contact points, and A denotes the cross sectional area (or effective thickness) of the film. This means if A decreases because of the formation of the junction and depletion layer, then R will increase. In case of bare ZnO, the surface resistance was ∼130 kΩ. For the coating of 5 nm Pd−Ag layer on ZnO, the resistance was about 150 kΩ. The increment of resistance was due to the formation of depletion region at the metal-semiconductor junction. However, only ∼40% response towards test gas was found for such pattern, might be due to the coverage of ZnO layer by Pd−Ag and subsequent lowering of the active surface to volume ratio of ZnO film. For 1 nm Pd−Ag layer, comparatively higher resistance (∼180 kΩ) was observed, with partial coverage of the lower lying ZnO film (Figure 2b). This in turn increases the number of active ZnO sites, in which O_2 and the test gas get adsorbed. The adsorbed O_2 on the surface forms O_2^- at 100°C, which creates space charge regions on those parts of the ZnO surface. The increase in the initial resistance for this pattern is not only due to the depletion region but also due to the space charge region created by O_2^- ions on the ZnO surface. The gas response was somewhat increased (total 50%) in comparison to the 5 nm layer, because of the increase in the number of active ZnO sites opened up due to partial covering by 1 nm Pd−Ag layer. In the case of Pd−Ag dotted structure, the initial resistance was found to be much higher (∼250 kΩ) than the other two patterns, as most of the ZnO surface was bare which can interact with molecular O_2 to form O_2^- (at 100 °C) and creates a large number of space charge region. Also the Pd−Ag dots on ZnO create Schottky barrier and depletion region in the interfaces, however, the effect due to space charge region is predominating here. Because of the combined effect, a high resistance of about 250 kΩ was found in this case. Also the response was highest for Pd−Ag dotted structure (about 80%), because in this case the active surface to volume ratio of ZnO reached its highest position because the minimal coverage by Pd−Ag. The entire phenomena can be explained using Scheme 5.

4. CONCLUSIONS

Fabrication of Pd−Ag alloy activated ZnO thin film based highly selective methane sensor prototype has been reported. Among the three possible Pd−Ag sensitizer patterns, the dotted structure was found to be most efficient for selective methane sensing at comparatively low operating temperature (100 °C).

dx.doi.org/10.1021/am404883x | ACS Appl. Mater. Interfaces 2014, 6, 3879−3887

The role of Pd−Ag activation, adsorbed O_2 molecules and its derivatives (O_2^- and O^-) towards the sensitivity and selectivity of methane have been explained. We have also showed that the selectivity is dependent on the electronic band structure of the activated ZnO films. The sensor performance was found to be sufficiently stable with consistent selectivity over a broad range of concentrations of the three test gases. A comparison on methane selectivity has been made with one of the commercially available sensors, and our reported prototype came out with better result.

■ ASSOCIATED CONTENT

Supporting Information

Detailed information about the sensor. This material is available free of charge via the Internet at http://pubs.acs.org.

■ AUTHOR INFORMATION

Corresponding Authors

*E-mail: sahahiran@gmail.com.
*E-mail: nilsci@yahoo.co.uk.

Notes

The authors declare no competing financial interest.

■ REFERENCES

(1) Wan, Q.; Li, Q.H.; Chen, Y. J.; Wang, T. H.; He, X. L.; Li, J. P.; Lin, C. L. *Appl. Phys. Lett.* **2004**, *84*, 3654−3656.
(2) Li, C. C.; Du, Z. F.; Li, L. M.; Yu, H. C.; Wan, Q.; Wang, T. H. *Appl. Phys. Lett.* **2007**, *91*, No. 032101.
(3) Kim, Y. S.; Ha, S. C.; Kim, K. W.; Yang, H. S.; Choi, S. Y.; Kim, Y. T.; Park, J. T.; Lee, C. H.; Choi, J. Y.; Park, J. S.; Lee, K. Y. *Appl. Phys. Lett.* **2005**, *86*, No. 213105.
(4) Yu, H. Y.; Kang, B. H.; Pi, U. H.; Park, C. W.; Choi, S. Y.; Kim, G. T. *Appl. Phys. Lett.* **2007**, *86*, No. 253102.
(5) Feng, P.; Wan, Q.; Wang, T. H. *Appl. Phys. Lett.* **2007**, *87*, No. 213111.
(6) Ismail, B.; Abaab, M.; Rezig, B. *Thin Solid Films* **2001**, *383*, 92−94.
(7) Hernandez-Ramirez, F.; Prades, J. D.; Morante, J. R. *Sens. Mater.* **2009**, *21*, 219−227.
(8) Xu, J. Q.; Chen, Y. P.; Chen, D. Y.; Shen, J. N. *Sens. Actuators B* **2006**, *113*, 526−531.
(9) Xi, Y.; Hu, C. G.; Han, X. Y.; Xiong, Y. F.; Gao, P. X.; Liu, G. B. *Solid State Commun.* **2007**, *141*, 506−509.
(10) Han, X. G.; He, H. Z.; Kuang, Q.; Zhou, X.; Zhang, X. H.; Xu, T.; Xie, Z. X.; Zheng, L. S. *J. Phys. Chem C* **2009**, *113*, 584−589.
(11) Wang, Y. D.; Zhang, S.; Ma, C. L.; Li, H. D. *J. Lumin.* **2007**, *126*, 661−664.
(12) Ueda, T.; Plashnitsa, V. V.; Nakatou, M.; Miura, N. *Electrochem. Commun.* **2007**, *9*, 197−200.
(13) Lim, H. J.; Lee, D. Y.; Oh, Y. J. *Sens. Actuators, A* **2006**, *125*, 405−410.
(14) Hsueh, T. J.; Hsu, C. L.; Chang, S. J.; Chen, I. C. *Sens. Actuators, B* **2007**, *126*, 473−477.
(15) Dikovska, A. Og.; Atanasov, P. A.; Tonchev, S.; Ferreira, J.; Escoubas, L. *Sens. Actuators, A* **2007**, *140*, 19−23.
(16) Bhattacharyya, P.; Mishra, G. P.; Sarkar, S. K. *Microelectron. Reliab.* **2011**, *51*, 2185−2194.
(17) Bhatlachaiyya, P.; Basu, P. K.; Mukherjee, N.; Mondal, A.; Saha, H.; Basu, S. *J. Mater. Sci.: -Mater. Electron.* **2007**, *18*, 823−829.
(18) Wang, J. X.; Sun, X. W.; Xie, S. S.; Yang, Y.; Chen, H. Y.; Lo, G. Q.; Kwong, D. L. *J. Phys. Chem. C* **2007**, *111*, 7671−7675.
(19) Wang, J. X.; Sun, X. W.; Huang, H.; Lee, Y. C.; Tan, O. K.; Yu, M. B.; Lo, G. Q.; Kwong, D. L. *Appl. Phys. A* **2007**, *88*, 611−615.
(20) Hsueh, T. J.; Chen, Y. W.; Chang, S. J.; Wang, S. F.; Hsu, C. L.; Lin, Y. R.; Lin, T. S.; Chen, I. C. *Sens. Actuators, B* **2007**, *125*, 498−503.
(21) Liu, R. L.; Xiang, Q.; Pan, Q. Y.; Cheng, Z. X.; Shi, L. Y.; Xuebao, W. C. *J. Inorg . Mater.* **2006**, *21*, 793−796.
(22) Kang, B. S.; Wang, H. T.; Tien, L. C.; Ren, F.; Gila, B. P.; Norton, D. P.; Abernathy, C. R.; Lin, J.; Pearton, S. J. *Sensors* **2006**, *6*, 643−666.
(23) Tang, H.; Yan, M.; Zhang, H.; Li, S.; Ma, X.; Wang, M.; Yang, D. *Sens. Actuators, B* **2006**, *114*, 910−915.
(24) Fryberger, T. B.; Semancik, S. *Sens. Actuators, B* **1990**, *2*, 305−309.
(25) Semancik, S.; Fryberger, T. B. *Sens. Actuators, B* **1990**, *1*, 97−02.
(26) Madler, L.; Roessler, A.; Pratsinis, S. E.; Sahm, T.; Gurlo, A.; Barsan, N.; Weimar, U. *Sens. Actuators, B* **2006**, *114*, 283−295.
(27) Choi, U. S.; Sakai, G.; Shimanoe, K.; Yamazoe, N. *Sens. Actuators, B* **2006**, *107*, 397−401.
(28) Kennedy, M. K.; Kruis, F. E.; Fissan, H.; Mentha, B. R.; Stappert, S.; Dumpich, G. *J. Appl Phys.* **2003**, *93*, 551−560.
(29) Joshi, R. K.; Kruis, F. E.; Dmitrieva, O. *J. Nanopart. Res.* **2006**, *8*, 797−808.
(30) Gong, J.; Chen, Q.; Lian, M. R.; Liu, N. C.; Stevenson, R. G.; Adami, F. *Sens. Actuators, B* **2006**, *114*, 32−39.
(31) Galdikas, A.; Mironas, A.; Setkus, A. *Sens. Actuators, B* **1995**, *26*, 29−32.
(32) Patil, S. B.; Patil, M. A.; More, P. P. *Sens. Actuators, B* **2007**, *125*, 126−130.
(33) Han, C. H.; Hong, D. U.; Gwak, J.; Han, S. D. *Korean J. Chem. Eng.* **2007**, *24*, 927−931.
(34) Moon, H. S.; Kim, S. E.; Choi, W. C. *Trans. Electr. Electron. Mater.* **2012**, *13*, 106−109.
(35) Mahmood, F. S.; Gould, R. D.; Hassan, A. K.; SAlih, H. M. *Thin Solid Films* **1995**, *270*, 376−379.
(36) Narayan, J.; Dovidenko, K.; Sharma, A. K.; Oktyabrsky, S. *J. Appl. Phys.* **1998**, *84*, 2597−2601.
(37) Yee, Y. E.; Lee, J. B.; Kim, Y. J.; Yang, H. K.; Park, J. C.; Kim, H. J. *J. Vac. Sci. Technol., A* **1996**, *14*, 1943−1949.
(38) Chang, P.; Fan, Z.; Wang, D.; Tseng, W.; Chiou, W.; Hong, J.; Lu, J. G. *Chem. Mater.* **2004**, *16*, 5133−5137.
(39) Haga, K.; Kamidaira, M.; Kashiwaba, Y.; Sekiguchi, T.; Watanabe, H. *J. Cryst. Growth* **2000**, *214/215*, 77−80.
(40) Park, D.; Tak, Y.; Yong, K. *J. Nanosci. Nanotechnol.* **2008**, *8*, 623−627.
(41) Yao, B. D.; Chan, Y. F.; Wang, N. *Appl. Phys. Lett.* **2007**, *81*, 757−759.
(42) Bethke, S.; Pan, H.; Wessels, B. W. *Appl. Phys. Lett.* **1988**, *52*, 138−140.
(43) Kuroyanagi, A. *Japanese J. Appl. Phys.* **1989**, *28*, 219−222.
(44) Craciun, V.; Elders, J.; Gardeniers, J. G. E.; Boyd, I. W. *Appl. Phys. Lett.* **1994**, *65*, 2963−2965.
(45) Sakohara, S.; Ticanen, L. D.; Anderson, M. A. *J. Phys. Chem.* **1992**, *96*, 11086−11091.
(46) Hoyer, P.; Weller, H. *Chem. Phys. Lett.* **1994**, *221*, 379−384.
(47) Haase, M.; Weller, H.; Henglein, A. *J. Phys. Chem.* **1988**, *92*, 482−487.
(48) Dong, L. F.; Cui, Z. L.; Zhang, Z. K. *Nanostruct. Mater.* **1997**, *8*, 815−823.
(49) Mondal, A.; Mukherjee, N.; Bhar, S.K. *Mater. Lett.* **2006**, *60*, 1748−1752.
(50) Mukherjee, N.; Ahmed, Sk. F.; Chattopadhyay, K. K.; Mondal, A. *Electrochim. Acta.* **2009**, *54*, 4015−4024.
(51) Kim, N. H.; Kim, G. J. *J. Nanosci. Nanotechnol.* **2007**, *7*, 3914−3916.
(52) Morrison, S. R. In *Semiconductor Sensors*, 1st ed.; Sze, S. M., Ed.;Wiley-Interscience: New York, 1994; Vol. *1*, p 383.
(53) Levine, J. D.; Mark, P. *Phys. Rev.* **1966**, *144*, 751−763.
(54) Chon, H.; Pajares, J. *J. Catal.* **1969**, *14*, 257−260.
(55) Lantto, V.; Romppainen, P. *Surf. Sci.* **1987**, *192*, 243−264.
(56) Basu, S.; Basu, P. K. *J. Sens.* **2009**, *10.1155*, No. 861968.
(57) Kim, J.; Yong, K. *J. Phys. Chem. C* **2011**, *115*, 7218−7224.
(58) Ju, S.; Kim, S.; Mohammadi, S.; Janes, D. B; Ha, Y. G.; Facchetti, A.; Marks, T. J. *Appl. Phys. Lett.* **2008**, *92*, No. 022104.

(59) Gu, D.; Dey, S. K.; Majhi, P. *Appl. Phys. Lett.* **2006**, *89*, No. 082907.
(60) Dweydari, A. W.; Mee, C. H. B. *Phys. Status Solidi A* **2006**, *27*, 223−230.